New Journal of Physics
The open-access journal for physics

Phase diagram of the t–U^2 Hamiltonian of the weak coupling Hubbard model

Takashi Yanagisawa[1,2]

[1] Condensed-Matter Physics Group, Nanoelectronics Research Institute, National Institute of Advanced Industrial Science and Technology (AIST) Central 2, 1-1-1 Umezono, Tsukuba 305-8568, Japan
[2] CREST, Japan Science and Technology Agency (JST), Kawaguchi, Saitama 332-0012, Japan
E-mail: t-yanagisawa@aist.go.jp

New Journal of Physics **10** (2008) 023014 (21pp)
Received 7 August 2007
Published 12 February 2008
Online at http://www.njp.org/
doi:10.1088/1367-2630/10/2/023014

Abstract. We determine the symmetry of Cooper pairs, on the basis of the perturbation theory in terms of the Coulomb interaction U, for the two-dimensional Hubbard model on the square lattice. The phase diagram is investigated in detail. The Hubbard model for small U is mapped on to an effective Hamiltonian with the attractive interaction using the canonical transformation: $H_{\rm eff} = {\rm e}^{S} H {\rm e}^{-S}$. The gap equation of the weak coupling formulation is solved without numerical ambiguity to determine the symmetry of Cooper pairs. The superconducting gap crucially depends on the position of the van Hove singularity. We show the phase diagram in the plane of the electron filling $n_{\rm e}$ and the next nearest-neighbor transfer t'. The d-wave pairing is dominant for the square lattice in a wide range of $n_{\rm e}$ and t'. The d-wave pairing is also stable for the square lattice with anisotropic t'. The three-band d–p model is also investigated, for which the d-wave pairing is stable in a wide range of $n_{\rm e}$ and $t_{\rm pp}$ (the transfer between neighboring oxygen atoms). In the weak coupling analysis, the second-neighbor transfer parameter $-t'$ could not be so large so that the optimum doping rate is in the range of $0.8 < n_{\rm e} < 0.85$.

Contents

1. Introduction

Since the discovery of high-temperature superconductors, the strongly correlated electron systems have been studied intensively. The effect of the strong correlation between the electrons is important for many quantum critical phenomena such as unconventional superconductivity (SC). High-temperature superconductors [1]–[3] as well as heavy fermions [4]–[7] are known as the typical correlated electron systems. These systems are modeled by the Hamiltonian with the electronic interaction of the on-site Coulomb repulsion. Recently, the mechanisms of SC in high-temperature superconductors have been extensively studied using the two-dimensional (2D) Hubbard model [8]–[16].

The SC of the Hubbard model has been questioned for many years. It is extremely difficult to show the existence of superconducting phase for the Hubbard model in a reasonable way. At present we cannot answer this long-standing question. Instead of examining the possibility of SC, it is possible to investigate possible symmetries of Cooper pairs for an effective Hamiltonian with the attractive interaction. For this purpose effective Hamiltonians have been obtained for the Hubbard model. The t–J model is the well-known effective Hamiltonian derived in the limit of the large on-site repulsion U, using the canonical transformation $H_{t-J} = \mathrm{e}^{S} H \mathrm{e}^{-S}$ with $S \propto t/U$. On the other hand, in the limit of small U, the perturbation theory also leads to an effective Hamiltonian with the attractive interaction [17]–[20], where we have $S \propto U/t$. The phase diagram with respect to the Cooper pair symmetry can be determined if we solve the gap equation.

We must notice that we should compare the energy with other electronic states to show that the superconducting state is indeed stable. For the half-filled band with vanishing $t' = 0$ in two space dimensions, the antiferromagnetic order parameter for small U is [21]

$$\Delta_{\mathrm{AF}} = \frac{8tc}{U} \exp\left(-\sqrt{\frac{4\pi^2 tc}{U}}\right), \tag{1}$$

where $c = 3 - \sqrt{3}$. It is, however, obvious that the antiferromagnetically ordered state is unstable away from half filling if the Coulomb repulsion U is small. Thus, we focus on the

case of small U for which we have also a merit that the gap equation is considerably simplified. The purpose of the paper is to determine the gap symmetry for the square lattice using the small-U gap equation derived for the effective Hamiltonian. Although the real SC in correlated electron systems should be described by a theory of strong-coupling SC, the phase diagram can be determined in detail using the weak coupling formulation. Precise calculations are sometimes not easy at low temperatures in the strong-coupling formulation due to the Matsubara frequency summation and the wave number summation. It is important to examine the detailed phase diagram for materials belonging to strongly correlated systems such as the cuprate high-temperature superconductors, the organic superconductors, the ruthenate superconductor Sr_2RuO_4.

The paper is organized as follows. In section 2, the effective Hamiltonian is derived using the canonical transformation. We show that we can derive the attractive effective Hamiltonian using some approximations. In section 3, the gap equation is shown and the results are presented in section 4. We give a summary in section 5.

2. Effective Hamiltonian

The Hubbard Hamiltonian is

$$H = -t \sum_{\langle ij\rangle\sigma} (c^{\dagger}_{i\sigma} c_{j\sigma} + \text{h.c.}) - t' \sum_{\ll j\ell \gg \sigma} (c^{\dagger}_{j\sigma} c_{\ell\sigma} + \text{h.c.}) + U \sum_{i} n_{i\uparrow} n_{i\downarrow}, \tag{2}$$

where $\langle ij\rangle$ and $\ll j\ell \gg$ denote the nearest-neighbor and next-nearest-neighbor pairs, respectively. U is the on-site Coulomb repulsion. The unit of energy is given by t in this paper. The total number of sites and the number of electrons are denoted as N and $N_{\rm e}$, respectively. The half-filled band corresponds to $n_{\rm e} = N_{\rm e}/N = 1$.

The effective Hamiltonian is derived using the perturbation theory for small U. The canonical transformation also maps the Hubbard model to an effective Hamiltonian with the attractive interaction [22]. Since no instability except SC occurs for small U away from half filling, we assume that the pairing interaction is the most singular. The procedure of mapping is as follows. The Hamiltonian is written as

$$H = H_0 + H_1 + H_2 + H_3, \tag{3}$$

where

$$H_0 = \sum_{k\sigma} \xi_k c^{\dagger}_{k\sigma} c_{k\sigma}, \tag{4}$$

$$H_1 = \frac{U}{N} \sum_{k\neq k'} c^{\dagger}_{k'\uparrow} c^{\dagger}_{-k'\downarrow} c_{-k\downarrow} c_{k\uparrow}, \tag{5}$$

$$H_2 = \frac{U}{N} \sum_{k\neq k', q\neq 0} c^{\dagger}_{k'\uparrow} c^{\dagger}_{-k'-q\downarrow} c_{-k-q\downarrow} c_{k\uparrow}, \tag{6}$$

$$H_3 = \frac{U}{N} \sum_{kk'} c^{\dagger}_{k\uparrow} c_{k\uparrow} c^{\dagger}_{k'\downarrow} c_{k'\downarrow}. \tag{7}$$

The dispersion relation ϵ_k for the square lattice is

$$\epsilon_k = -2t(\cos k_x + \cos k_y) - 4t' \cos k_x \cos k_y, \tag{8}$$

where μ is the chemical potential. We set $\xi_k = \epsilon_k - \mu$. Using a canonical transformation, $\tilde{\psi} = \mathrm{e}^S \psi$, we look for the solution of the Schrödinger equation $H_{\rm eff}\tilde{\psi} = E\tilde{\psi}$. The effective Hamiltonian reads

$$\begin{aligned} H_{\rm eff} = \mathrm{e}^S H \mathrm{e}^{-S} &= H + [S, H] + \tfrac{1}{2}[S, [S, H]] + \cdots \\ &= H_0 + H_1 + H_2 + H_3 + [S, H_0 + H_1 + H_2 + H_3] + \tfrac{1}{2}[S, [S, H_0]] + \cdots . \end{aligned} \tag{9}$$

We determine S so as to satisfy $H_2 + [S, H_0] = 0$. We find

$$S = \frac{U}{N} \sum_{k\neq k', q\neq 0} \frac{1}{\xi_{k'+q} + \xi_{k'} - \xi_{k+q} - \xi_k} c^\dagger_{k'\uparrow} c_{-k'-q\downarrow} c^\dagger_{-k-q\downarrow} c_{k\uparrow}. \tag{10}$$

Since $[S, H_3] = 0$, we obtain up to the order of U^2,

$$H_{\rm eff} = H_0 + H_1 + H_3 + [S, H_1] + \tfrac{1}{2}[S, H_2]. \tag{11}$$

The commutator $[S, H_2]$ is evaluated as

$$\begin{aligned} [S, H_2] = \left(\frac{U}{N}\right)^2 \sum_{k\neq k', q\neq 0} \sum_{p\neq p', q'\neq 0} S^q_{kk'} (&-\delta_{pk'} c^\dagger_{p'\uparrow} c^\dagger_{-p'-q'\downarrow} c_{-p-q'\downarrow} c^\dagger_{-k'-q\downarrow} c_{-k-q\downarrow} c_{k\uparrow} \\ &+\delta_{p+q', k'+q} c^\dagger_{p'\uparrow} c^\dagger_{-p'-q'\downarrow} c^\dagger_{k'\uparrow} c_{p\uparrow} c_{-k-q\downarrow} c_{k\uparrow} - \delta_{p'+q', k+q} c^\dagger_{k'\uparrow} c^\dagger_{-k'-q\downarrow} c^\dagger_{p'\uparrow} c_{k\uparrow} c_{-p-q'\downarrow} c_{p\uparrow} \\ &+\delta_{p'k} c^\dagger_{k'\uparrow} c^\dagger_{-k'-q\downarrow} c_{-k-q\downarrow} c^\dagger_{-p'-q'\downarrow} c_{-p-q'\downarrow} c_{p\uparrow}), \end{aligned} \tag{12}$$

where

$$S^q_{kk'} = \frac{1}{\xi_{k'+q} + \xi_{k'} - \xi_{k+q} - \xi_k}. \tag{13}$$

Since the purpose of this paper is to investigate the pairing symmetry, we need only the first term and the last term of $[S, H_2]$. We find that the average of the second and third terms with respect to the Bardeen–Cooper–Schrieffer (BCS) wavefunction vanish. Due to the same reason $[S, H_1]$ can be neglected. Then the effective Hamiltonian is

$$\begin{aligned} H_{t-U^2} = \sum_{k\sigma} \xi_k c^\dagger_{k\sigma} c_{k\sigma} + \frac{U}{N} \sum_{k\neq k'} c^\dagger_{k'\uparrow} c^\dagger_{-k'\downarrow} c_{-k\downarrow} c_{k\uparrow} + \frac{1}{2}\frac{U^2}{N^2} \sum_{k\neq k', q\neq 0} \sum_{p\neq p', q'\neq 0} \frac{1}{\xi_{k'+q} + \xi_{k'} - \xi_{k+q} - \xi_k} \\ \times (\delta_{p'k} c^\dagger_{k'\uparrow} c_{-k-q\downarrow} c^\dagger_{-k'-q\downarrow} c_{-p-q'\downarrow} c^\dagger_{-p'-q'\downarrow} c_{p\uparrow} - \delta_{pk'} c^\dagger_{p'\uparrow} c_{-p-q'\downarrow} c^\dagger_{-p'-q'\downarrow} c_{-k-q\downarrow} c^\dagger_{-k'-q\downarrow} c_{k\uparrow}). \end{aligned} \tag{14}$$

If we set $k = p + q'$ and $p' = k' + q$, the first term of $[S, H_2]$ is approximated as

$$\begin{aligned} H_{2a} \equiv -\left(\frac{U}{N}\right)^2 &\sum_{k\neq k', q\neq 0} \sum_{p\neq p', q'\neq 0} S^q_{k'k} \delta_{pk'} c^\dagger_{p'\uparrow} c^\dagger_{-p'-q'\downarrow} c_{-p-q'\downarrow} c^\dagger_{-k'-q\downarrow} c_{-k-q\downarrow} c_{k\uparrow} \\ &\approx \left(\frac{U}{N}\right)^2 \sum_{k\neq k', q\neq 0} c^\dagger_{k'+q\uparrow} c^\dagger_{-k'-q\downarrow} \frac{c^\dagger_{-k-q\downarrow} c_{-k-q\downarrow}}{\xi_{k'+q} + \xi_{k'} - \xi_{k+q} - \xi_k} c_{-k\downarrow} c_{k\uparrow} \\ &\approx \left(\frac{U}{N}\right)^2 \sum_{k\neq k'-q, q\neq 0} c^\dagger_{k'\uparrow} c^\dagger_{-k'\downarrow} \frac{f_{-k-q}}{\xi_{k'} + \xi_{k'-q} - \xi_{k+q} - \xi_k} c_{-k\downarrow} c_{k\uparrow} \\ &= \left(\frac{U}{N}\right)^2 \sum_{k'+q\neq 0, k+q\neq 0} c^\dagger_{k'\uparrow} c^\dagger_{-k'\downarrow} \frac{f_q}{\xi_{k'+k+q} - \xi_{-q} + \xi_{k'} - \xi_k} c_{-k\downarrow} c_{k\uparrow}, \end{aligned} \tag{15}$$

where f_k is the Fermi distribution function,

$$f_k = \frac{1}{e^{\beta\xi_k}+1}. \tag{16}$$

Since the summation is restricted to the small region near the Fermi surface, we obtain assuming $\xi_{-k} = \xi_k$

$$H_{2a} \approx \left(\frac{U}{N}\right)^2 \sum_{k\neq -q, k'\neq -q} \frac{f_q}{\xi_{k'+k+q} - \xi_q} c^\dagger_{k'\uparrow} c^\dagger_{-k'\downarrow} c_{-k\downarrow} c_{k\uparrow}. \tag{17}$$

Similarly the last term of $[S, H_2]$ is written as

$$H_{2b} \approx \left(\frac{U}{N}\right)^2 \sum_{k\neq -q, k'\neq -q} \frac{f_{k'+k+q}}{\xi_{k'+k+q} - \xi_q} c^\dagger_{k'\uparrow} c^\dagger_{-k'\downarrow} c_{-k\downarrow} c_{k\uparrow}. \tag{18}$$

The resulting effective Hamiltonian is

$$H_{\text{eff}} = e^S H e^{-S} \equiv H_{t-U^2} = \sum_{k\sigma} \xi_k c^\dagger_{k\sigma} c_{k\sigma} + \sum_{kk'} V_{kk'} c^\dagger_{k'\uparrow} c^\dagger_{-k'\downarrow} c_{-k\downarrow} c_{k\uparrow}, \tag{19}$$

where

$$V_{kk'} = \frac{U}{N} + \frac{U^2}{N}\chi(\mathbf{k}+\mathbf{k}'). \tag{20}$$

$\chi(\mathbf{k}+\mathbf{k}')$ is the magnetic susceptibility defined as

$$\chi(\mathbf{k}+\mathbf{k}') = \frac{1}{N}\sum_q \frac{f_{k+k'+q} - f_q}{\xi_q - \xi_{k+k'+q}}. \tag{21}$$

Thus, we have reached the effective Hamiltonian up to the order of U^2 using the canonical transformation.

3. Gap equation

The gap equation for the t–U^2 model was investigated in [19]. Since the equation was considerably simplified for small U, the gap equation was solved without numerical ambiguity. We define the order parameter,

$$\Delta_k = \sum_{k'} V_{kk'} \langle c_{-k'\downarrow} c_{k'\uparrow} \rangle. \tag{22}$$

Using the mean-field theory, the gap equation for the Hamiltonian H_{t-U^2} is

$$\Delta_k = -\sum_{k'} V_{kk'} \Delta_{k'} \frac{1 - 2f(E_{k'})}{2E_{k'}}, \tag{23}$$

where $E_k = \sqrt{\xi_k^2 + \Delta_k^2}$. We assume the anisotropic order parameter given as

$$\Delta_{\mathbf{k}} = \Delta \cdot z_{\mathbf{k}}, \tag{24}$$

where $z_{\mathbf{k}}$ denotes the $\mathbf{k}$-dependence of $\Delta_{\mathbf{k}}$. At $T = 0$, the gap equation is written as

$$\Delta_k = -\frac{1}{2}\sum_{k'} V_{kk'} \frac{\Delta_{k'}}{E_{k'}}. \tag{25}$$

For small U, the gap equation for anisotropic pairing is extremely simplified retaining only the logarithmic term [19]:

$$z_k = \log\left(\frac{\Delta}{2\omega_0}\right) U^2 \frac{1}{N} \sum_{k'} \chi(\mathbf{k}+\mathbf{k}')\delta(\xi_{k'}) z_{k'}, \tag{26}$$

where ω_0 is the cut-off energy. The critical temperature T_c is determined by

$$z_{\mathbf{k}} = -\sum_{\mathbf{k}'} V_{\mathbf{k}\mathbf{k}'} z_{\mathbf{k}'} \frac{1-2f(|\xi_{\mathbf{k}'}|)}{2|\xi_{\mathbf{k}'}|} \quad \text{for } T = T_c. \tag{27}$$

For small U, the critical temperature T_c is extremely small. In this case, we can use the following approximation,

$$\begin{aligned} I &\equiv \int_0^{\omega_0} \mathrm{d}\xi g(\xi) \frac{\tanh(\beta_c \xi/2)}{\xi} \\ &\approx g(\omega_0)\log\omega_0 - \frac{\beta_c}{2}\int_0^{\omega_0} \mathrm{d}\xi \log\xi g(\xi) \frac{1}{(\cosh(\beta_c\xi/2))^2} \\ &= g(\omega_0)\log\omega_0 - \int_0^{\beta_c\omega_0/2} \mathrm{d}x \log\left(\frac{2x}{\beta_c}\right) g\left(\frac{2x}{\beta_c}\right) \frac{1}{(\cosh x)^2} \\ &= g(\omega_0)\log\omega_0 - g(0)\int_0^{\beta_c\omega_0/2} \mathrm{d}x \log\left(\frac{2x}{\beta_c}\right) \frac{1}{(\cosh x)^2} \\ &\approx g(0)\log\left(\frac{2\mathrm{e}^{\gamma}\omega_0}{\pi k_B T_c}\right), \end{aligned} \tag{28}$$

where we assume that $g(\xi)$ is a slowly varying function and $g'(\xi)$ is negligible. The equation is written as

$$z_{\mathbf{k}} = -\log\left(\frac{2\mathrm{e}^{\gamma}\hbar\omega_0}{\pi k_B T_c}\right) \sum_{\mathbf{k}'} V_{\mathbf{k}\mathbf{k}'} z_{\mathbf{k}'} \delta(\xi_{\mathbf{k}'}). \tag{29}$$

Since T_c is very small, the summation over $\mathbf{k}'$ can be restricted to the average over near the Fermi surface. If we solve the eigenequation

$$\frac{2}{N}\sum_{\mathbf{k}'} \chi(\mathbf{k}+\mathbf{k}') z_{\mathbf{k}'} \delta(\xi_{\mathbf{k}'}) = -x z_{\mathbf{k}}, \tag{30}$$

the critical temperature is obtained as

$$k_B T_c = 1.13\omega_0 \exp\left(-\frac{2t^2}{xU^2}\right), \tag{31}$$

where the energy unit is given by t. Since Δ is given as

$$\Delta = 2\omega_0 \exp\left(-\frac{2t^2}{xU^2}\right), \tag{32}$$

the ratio $2\Delta/k_B T_c$ equals the BCS universal value $2\pi/\mathrm{e}^{\gamma} = 3.53$.

4. Pairing symmetry

4.1. Method of solving the eigenvalue equation

We express z_k and $V_{kk'}$ in terms of the polar coordinates [19]:

$$z_k = z(\xi, \theta), \tag{33}$$

$$\chi(\mathbf{k}+\mathbf{k}') = \chi(\xi, \theta, \xi', \theta'), \tag{34}$$

where $\mathbf{k}$ is expressed using the polar angle θ: $\mathbf{k} = (\xi, \theta)$ in terms of the polar coordinates. We consider the gap function on the Fermi surface $z(\theta) \equiv z(0, \theta)$. If we define $\chi(\theta, \theta') = \chi(0, \theta, 0, \theta')$, the gap equation is

$$2\int_0^{2\pi} \mathrm{d}\theta' \rho_{\mathrm{F}}(\theta')\chi(\theta, \theta')z(\theta') = -xz(\theta), \tag{35}$$

where $\rho_{\mathrm{F}}(\theta)$ is the density of states at the Fermi surface:

$$\rho_{\mathrm{F}}(\theta) = \frac{1}{(2\pi)^2} k_{\mathrm{F}}(\theta) \frac{1}{|(\partial\xi/\partial k)(k = k_{\mathrm{F}}(\theta))|}, \tag{36}$$

where $k_{\mathrm{F}}(\theta)$ is the Fermi wave number of the polar coordinate θ and $\partial\xi/\partial k$ is the derivative with respect to $k = |\mathbf{k}|$. If we expand $z(\theta)$ as

$$z(\theta) = \sum_n z_n \mathrm{e}^{\mathrm{i}n\theta}, \tag{37}$$

the gap equation is given as

$$\sum_n \chi_{mn} z_n = -xz_m, \tag{38}$$

where χ_{mn} are the matrix elements of $\chi(\theta, \theta')$:

$$\chi_{mn} = \frac{1}{\pi}\int_0^{2\pi} \mathrm{d}\theta\, \mathrm{d}\theta' \rho_{\mathrm{F}}(\theta')\mathrm{e}^{-\mathrm{i}m\theta}\chi(\theta, \theta')\mathrm{e}^{\mathrm{i}n\theta'}. \tag{39}$$

The number of basis functions kept in solving the eigenequation is 30–40 in this paper. The $\mathbf{k}$-space is divided into 200×20 points on equally spaced mesh in the numerical calculations of $\chi(\theta, \theta')$.

4.2. Simple square lattice

Let us investigate the phase diagram for the square lattice (figure 1). The basis functions $\{\mathrm{e}^{\mathrm{i}n\theta}\}$ ($n = 0, \pm1, \pm2, \ldots$) are classified into irreducible representations according to the symmetry group. The eigenfunctions are specified by one of irreducible representations of the square lattice (see table 1). It is convenient to use real basis functions $\cos(n\theta)$ and $\sin(n\theta)$ for this purpose. The gap function in each representation is [19]

$$z(\theta) = \sum_{\ell=1} z_{4\ell}\cos(4\ell\theta) \quad \mathrm{A}_1, \tag{40}$$

$$z(\theta) = \sum_{\ell=1} z_{4\ell}\sin(4\ell\theta) \quad \mathrm{A}_2, \tag{41}$$

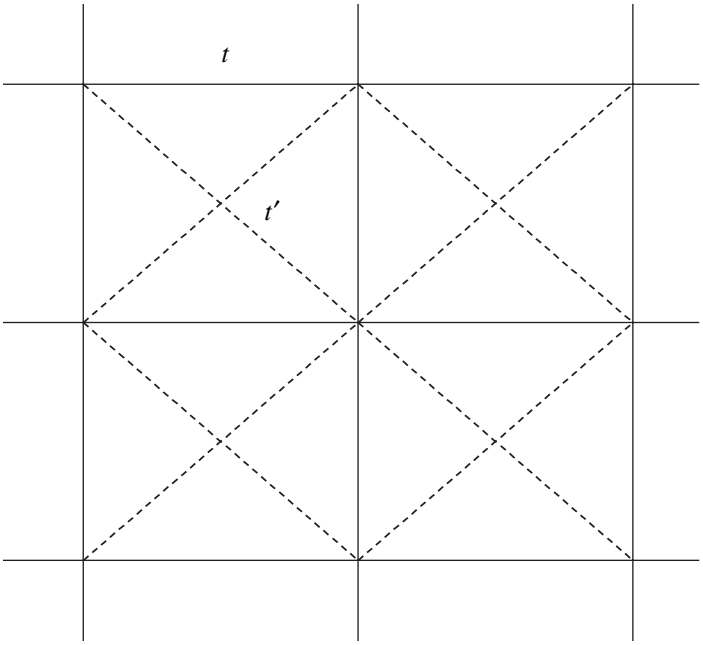

Figure 1. Square lattice with next-nearest transfer t'.

$$z(\theta) = \sum_{\ell=1} z_{4\ell-2}\cos(4\ell-2)\theta \quad \mathrm{B}_1, \tag{42}$$

$$z(\theta) = \sum_{\ell=1} z_{4\ell-2}\sin(4\ell-2)\theta \quad \mathrm{B}_2. \tag{43}$$

$$z(\theta) = \sum_{\ell=1} z_{2\ell-1}\cos(2\ell-1)\theta \quad \mathrm{E}. \\ \text{or } \sin(2\ell-1)\theta \tag{44}$$

In [19], the representations A_1–B_2 were investigated. Here, the E symmetry for triplet pairing is also examined. The eigenequation is solved for the above shown basis functions in the space of each irreducible representation. The eigenvalue x for $t' = 0$ is shown in figure 2 as a function of the electron density n_e. For $n_e > 0.6$ the paired state with $d_{x^2-y^2}$ symmetry is most stable for $t' = 0$. Since the exponent x sensitively depends on the van Hove singularity, x is an increasing function of n_e near half filling for $t' = 0$.

The exponent x for $t' = -0.1$, -0.2 and -0.3 is shown in figures 3–5, respectively. The exponents for small electron filling are not shown here because the high numerical accuracy is required for exponentially small exponents. As is shown in the figures, the d-wave state is most stable near half-filled case for t' in the range of $0 \leqslant t' \leqslant 0.4$. The position of the van Hove singularity depends on t', and the peak of x shifts as $-t' > 0$ increases (figure 6). x has a sharp peak showing a logarithmic increase due to the van Hove singularity:

$$x \sim -\log|\mu - \mu_{\mathrm{vH}}|, \tag{45}$$

where μ_{vH} is the chemical potential corresponding to the van Hove singularity. The figure suggests higher T_c for small $-t'$. The antiferromagnetism, however, may compete and suppress

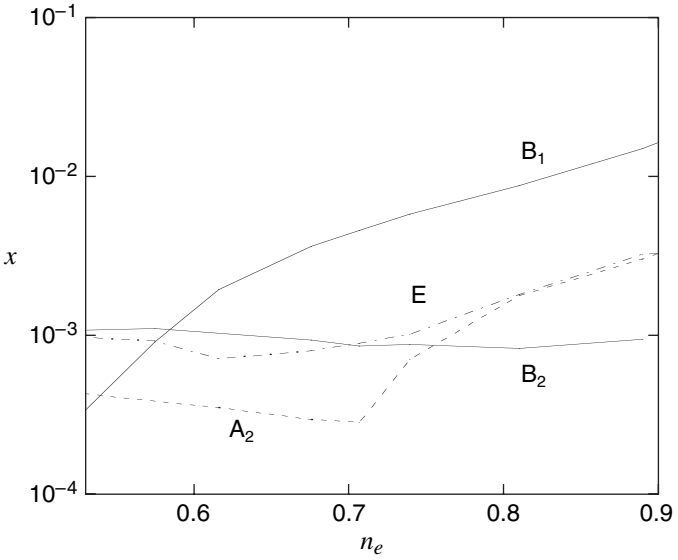

Figure 2. The exponent x as a function of the electron density for $t' = 0$. (See [19]. We have included x for the E representation.) Since the line for A_1 mostly coincides with that for B_2, the A_1 line is omitted.

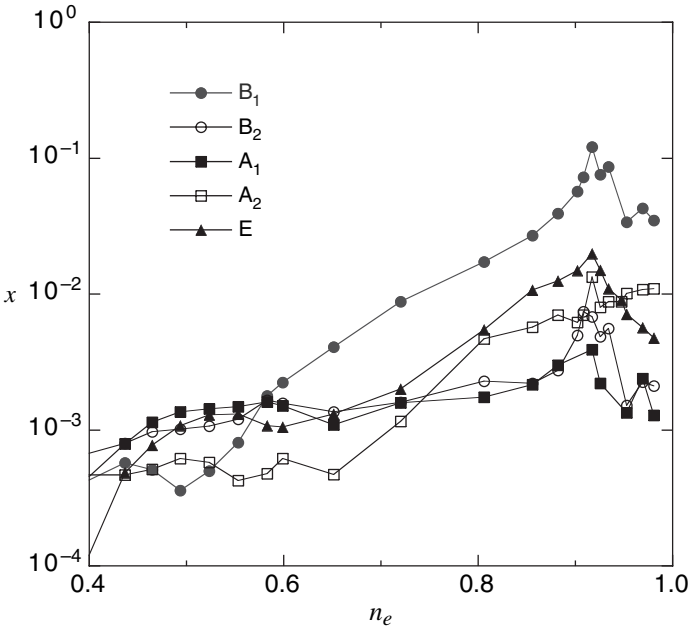

Figure 3. The exponent x as a function of the electron density for $t' = -0.1$.

SC near half filling. Hence, we must have a bell-shape critical temperature as a function of the electron filling.

It was pointed out from the electronic states calculations that the Fermi surface is much deformed for $Tl_2Ba_2CuO_6$ [23] and $HgBa_2CuO_4$ [24] for which the band parameter values must be assigned as $t' \sim -0.4$ and $t'' \sim 0.1$ (third-neighbor transfer). $Bi_2Sr_2CaCu_2O_{8+\delta}$ (Bi2212) also

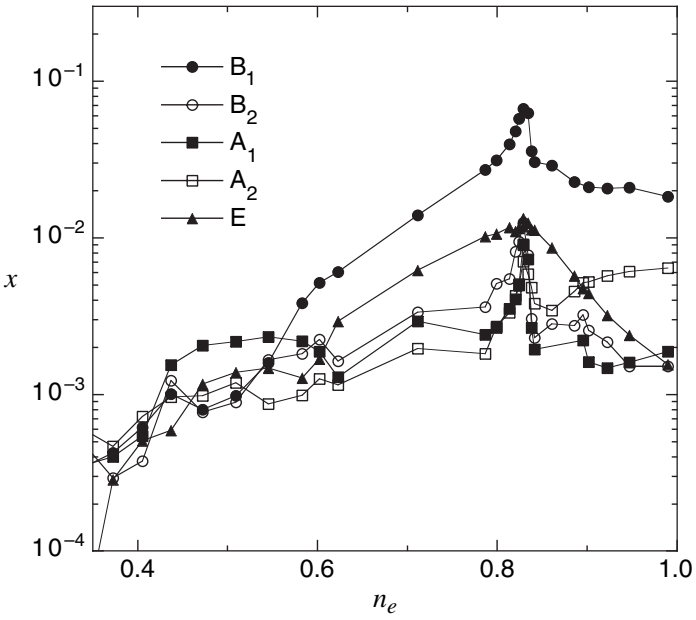

Figure 4. The exponent x as a function of the electron density for $t' = -0.2$.

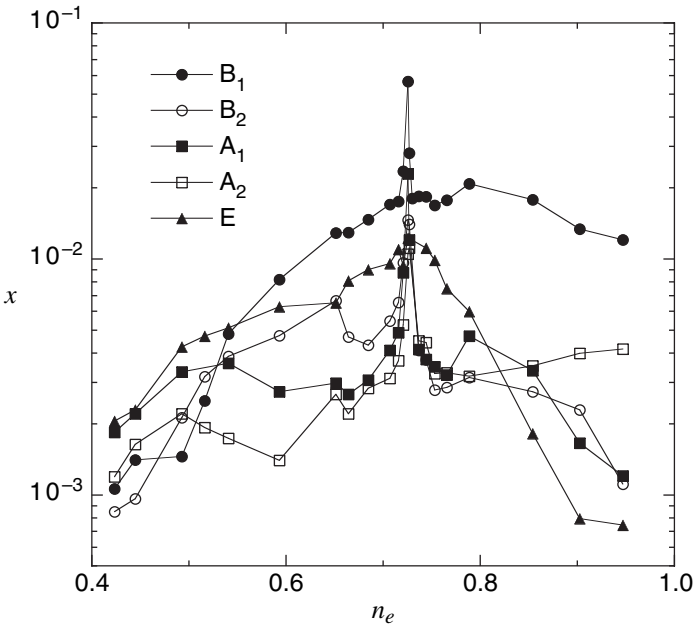

Figure 5. The exponent x as a function of the electron density for $t' = -0.3$.

has deformed Fermi surface so that $t' \sim -0.3$ and $t'' \sim 0.2$ [25]. For these values the optimum doping rate must be larger than that for $La_{1-x}Sr_xCuO_4$ (LSCO) for which $t' \sim -0.1$ and $t'' \sim 0$. Experiments, however, indicated that the optimum doping rate is almost the same for Bi2212 and LSCO [26]. This may be a flaw of the weak coupling formulation, which, however, may not be completely remedied by the strong coupling treatment since the van Hove singularity still has a large effect on the critical temperature. This suggests that we must re-examine the structure of

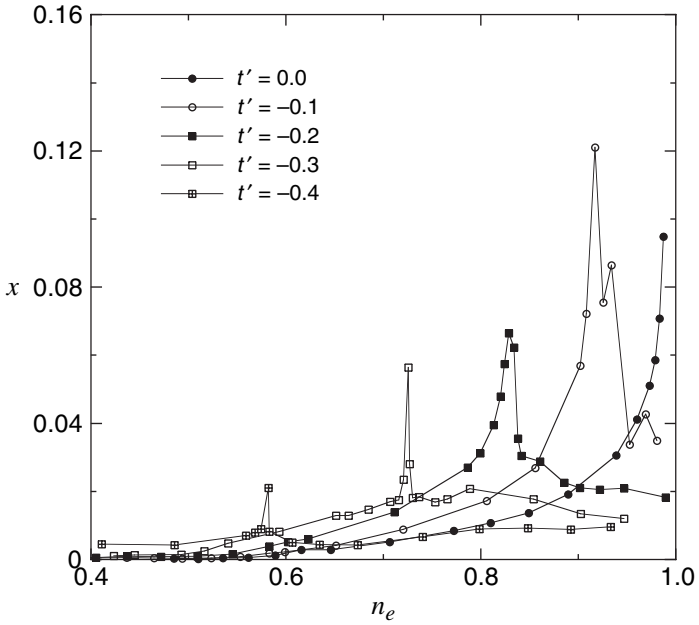

Figure 6. The exponent x of B_1 symmetry as a function of the electron density for $t' = 0$, -0.1, -0.2, -0.3 and -0.4.

the Fermi surface of high-temperature cuprates. In particular, the band parameters for Bi2212 will be modified if we take into account the double layer structure [27, 28]. The band structure reported by recent studies [28, 29] is well fitted using smaller t' such as [30][3]

$$t' \sim -0.2. \tag{46}$$

The phase diagram in the n_e–t' plane is shown in figure 7 for $t' \leqslant 0$ and in figure 8 for $t' \geqslant 0$. For $n_e \sim 0.5$ and $-t' \sim 0.4$, there is a possibility that the p-wave SC is realized. For example, the ruthenate superconducting material Sr_2RuO_4 [31] is sometimes modeled by the one-band Hubbard model for the γ orbital with $t' \sim -0.4$ and $n_e \simeq 0.67$ after the electron–hole transformation. The state of these parameters just corresponds to the point within the singlet region near the boundary to p-wave regions in figure 7. In order to obtain the stable p-wave pairing for the parameters corresponding to Sr_2RuO_4, we may need to consider the multi-band structure including α and β orbitals [32]. For $t' > 0$, we have a large d-wave region.

If t' is large and negative, i.e. if $-t' > 0.5$, we have the case with two Fermi surfaces; one is a large Fermi surface (FS1) and the other is a small Fermi surface (FS2) inside of the larger one. In this case, we must examine the coupled equation of two gap functions z_k^1 and z_k^2 corresponding to two Fermi surfaces:

$$\frac{2}{N}\sum_{\mathbf{k}':\mathrm{FS1}} \chi^{11}(\mathbf{k}+\mathbf{k}')z^1_{\mathbf{k}'}\delta(\xi_{\mathbf{k}'}) + \frac{2}{N}\sum_{\mathbf{k}':\mathrm{FS2}} \chi^{12}(\mathbf{k}+\mathbf{k}')z^2_{\mathbf{k}'} = -xz^1_{\mathbf{k}}, \tag{47}$$

$$\frac{2}{N}\sum_{\mathbf{k}':\mathrm{FS1}} \chi^{21}(\mathbf{k}+\mathbf{k}')z^1_{\mathbf{k}'}\delta(\xi_{\mathbf{k}'}) + \frac{2}{N}\sum_{\mathbf{k}':\mathrm{FS2}} \chi^{22}(\mathbf{k}+\mathbf{k}')z^2_{\mathbf{k}'} = -xz^2_{\mathbf{k}}, \tag{48}$$

[3] We thank K Yamaji for stimulating discussions on this point.

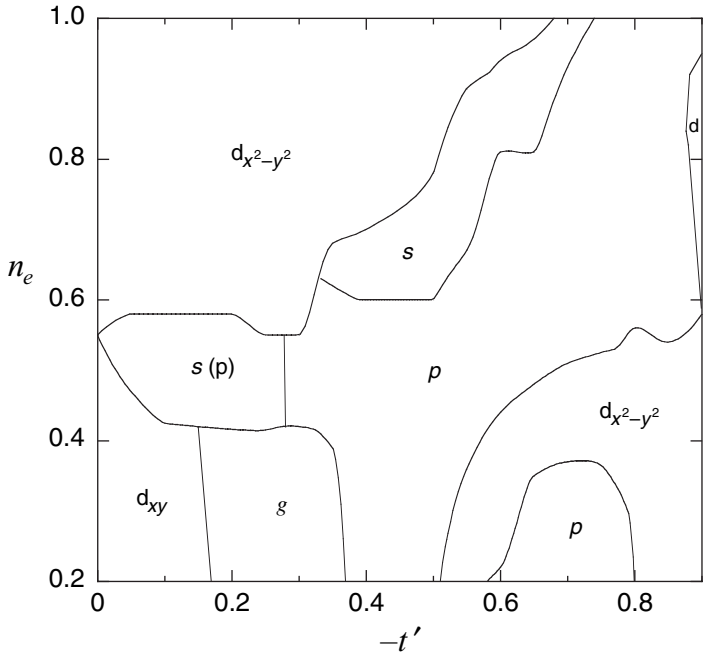

Figure 7. Phase diagram in the n_e-t' plane for $t' \leqslant 0$. *s* denotes the pairing state with extended, s-wave symmetry. In the s-wave region for small $|t'|$, the s- and p-wave states are sometimes nearly degenerate. Small regions near boundaries are not shown.

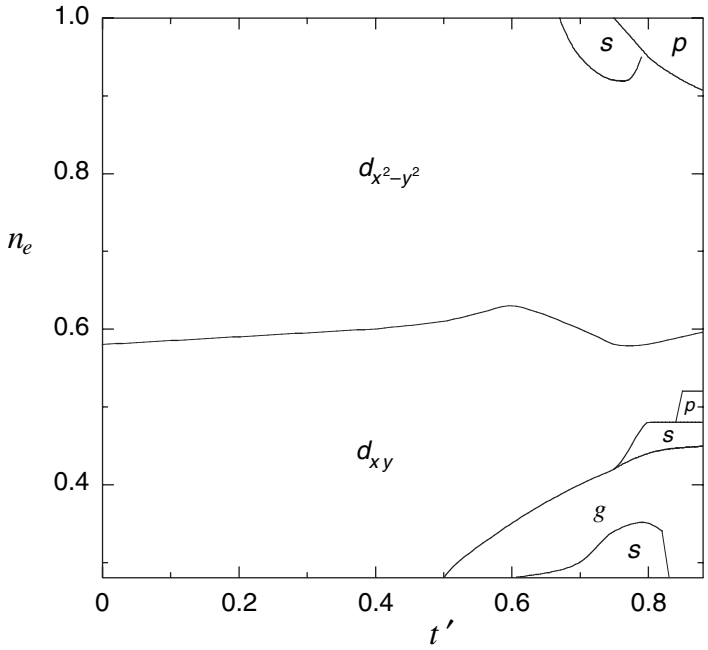

Figure 8. Phase diagram in the n_e-t' plane for $t' \geqslant 0$. s, g and d pairing states are almost degenerate in the low carrier region for large t'.

Table 1. Irreducible representations of C_{4v} for the square lattice. One of basis functions are also shown.

Representation	Symmetry	Bases		
A_1	s	1		$\cos(4\theta)$
A_2	g		$xy(x^2-y^2)$	$\sin(4\theta)$
B_1	$d_{x^2-y^2}$	$\cos(k_x)-\cos(k_y)$	x^2-y^2	$\cos(2\theta)$
B_2	d_{xy}	$\sin(k_x)\sin(k_y)$	xy	$\sin(2\theta)$
E	p	$\sin(k_x)$, $\sin(k_y)$	x, y	$\cos(\theta)$, $\sin(\theta)$

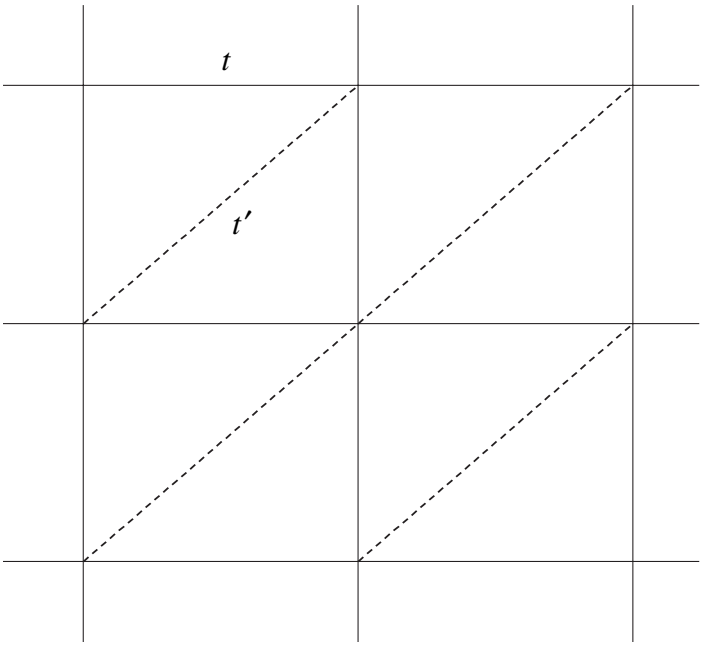

Figure 9. Square lattice with anisotropic next-nearest transfer t' (anisotropic triangular lattice) which is the lattice of organic conductors.

where the symbol $\sum_{k':FSi}$ indicates the summation over the Fermi surface FSi and $\chi^{ij}(\mathbf{k}+\mathbf{k}')$ is the susceptibility for $\mathbf{k}$ on FSi and $\mathbf{k}'$ on FSj. The stable pairing symmetry is also obtained using the electron–hole transformation for $t' > 0$ for which we have almost only one Fermi surface even in the electron-doped case.

4.3. Square lattice with anisotropic t'

The Hubbard model on the square lattice with anisotropic next-nearest-neighbor transfer t' (figure 9) has been investigated intensively as a model for organic conductors such as BDET-TTF(ET) molecules [33]–[35]. The model for organic conductors is well known as the Hubbard model with anisotropic next-nearest-neighbor transfer t' (which is sometimes called the anisotropic triangular lattice). The dispersion relation is

$$\xi_k = -2t(\cos k_x + \cos k_y) - 2t'\cos(k_x + k_y) - \mu. \tag{49}$$

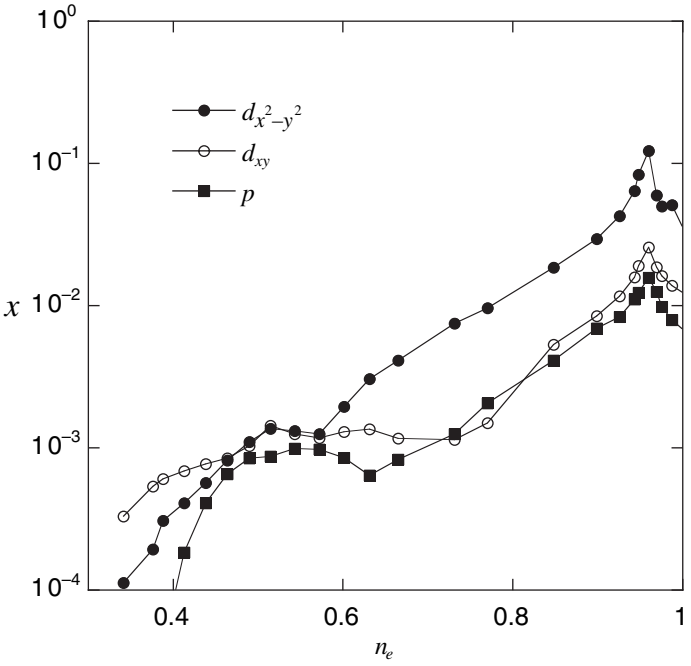

Figure 10. The exponent x on the square lattice with anisotropic $t' = -0.1$.

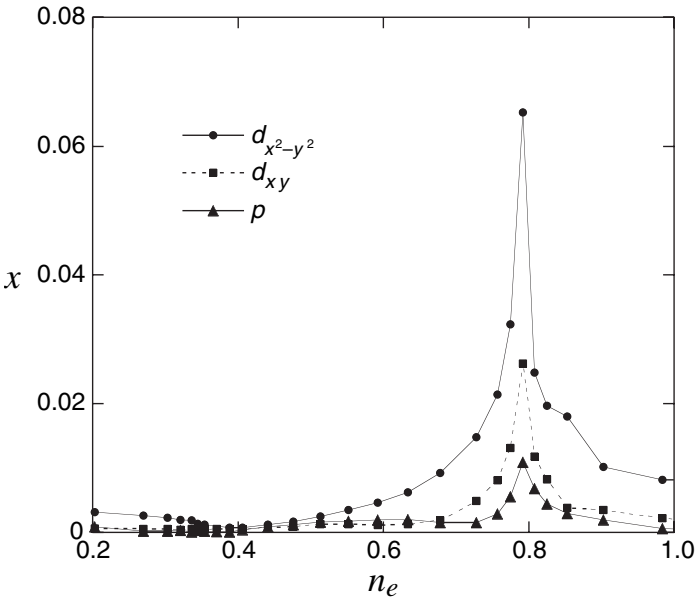

Figure 11. The exponent x on the square lattice with anisotropic $t' = -0.5$.

This model has the two-fold rotational symmetry and we classify the irreducible representation using the C_{2v} point group (table 2). The exponent x is in figures 10 and 11 as a function of the electron density n_e for $t' = -0.1$ and $t' = -0.5$, respectively. As apparent from the figures, the d-wave state is stable over the whole region, which is consistent with the FLEX prediction [36]. The phase diagram in the n_e–t' plane is presented in figure 12 for $t' < 0$ and in figure 13 for $t' > 0$. For this model, we conclude that the d-wave pairing is stable over the whole range of parameters.

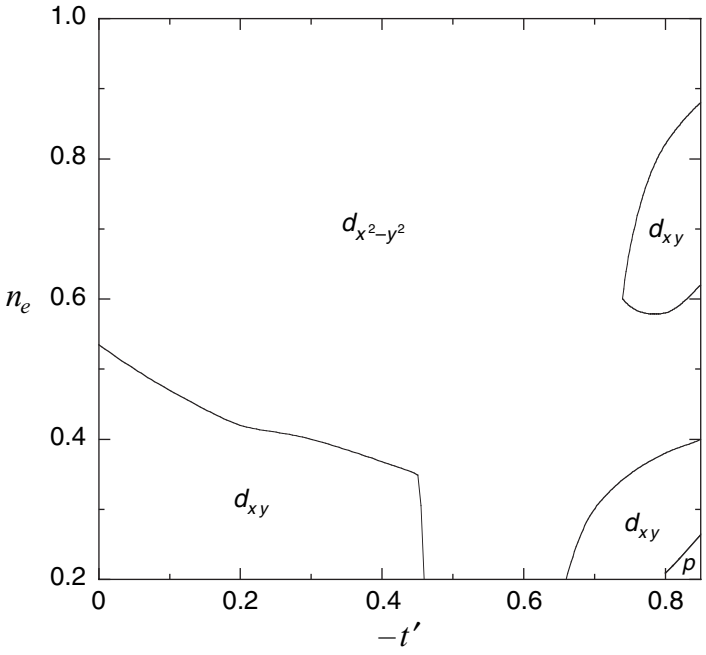

Figure 12. Phase diagram for the square lattice with anisotropic $t' < 0$ (lattice of organic conductors).

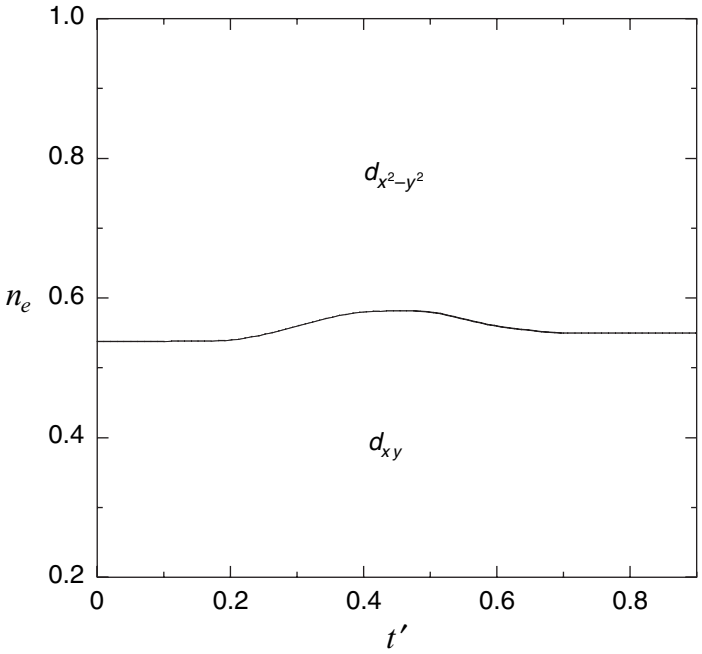

Figure 13. Phase diagram for the square lattice with anisotropic $t' > 0$ (lattice of organic conductors).

Table 2. Irreducible representations of C_{2v} for the square lattice with anisotropic next-nearest-neighbor transfer.

Representation	Symmetry	Bases	
A_1	$d_{x^2-y^2}$	x^2, y^2	$\cos(2\theta)$
A_2	d_{xy}	xy	$\sin(2\theta)$
B_1	p_x	x	$\cos(\theta)$
B_2	p_y	y	$\sin(\theta)$

4.4. Three-band d–p model

The formulation is also applied to the three-band model for the CuO_2 plane [37]. We are interested in the relation between the single-band Hubbard model and the three-band d–p model. The pairing symmetry in the electron-doped cuprates is still controversial between the d-wave and s-wave order parameter [38]–[40]. The Hamiltonian is

$$\begin{aligned} H_{\rm dp} = {} & \epsilon_{\rm d} \sum_{i\sigma} d^\dagger_{i\sigma} d_{i\sigma} + \epsilon_{\rm p} \sum_{i\sigma} (p^\dagger_{i+\hat{x}/2\sigma} p_{i+\hat{x}/2\sigma} + p^\dagger_{i+\hat{y}/2\sigma} p_{i+\hat{y}/2\sigma}) \\ & + t_{\rm dp} \sum_{i\sigma} [d^\dagger_{i\sigma} (p_{i+\hat{x}/2\sigma} + p_{i+\hat{y}/2\sigma} - p_{i-\hat{x}/2\sigma} - p_{i-\hat{y}/2\sigma}) + \text{h.c.}] \\ & + t_{\rm pp} \sum_{i\sigma} [p^\dagger_{i+\hat{y}/2\sigma} p_{i+\hat{x}/2\sigma} - p^\dagger_{i+\hat{y}/2\sigma} p_{i-\hat{x}/2\sigma} - p^\dagger_{i-\hat{y}/2\sigma} p_{i+\hat{x}/2\sigma} \\ & + p^\dagger_{i-\hat{y}/2\sigma} p_{i-\hat{x}/2\sigma} + \text{h.c.}] + U_{\rm d} \sum_i d^\dagger_{i\uparrow} d_{i\uparrow} d^\dagger_{i\downarrow} d_{i\downarrow}. \end{aligned} \tag{50}$$

In this subsection, the energy is measured in units of $t_{\rm dp}$. The energy levels of the non-interacting Hamiltonian is written as in a concise form [37]:

$$\epsilon^\alpha_{\mathbf{k}} = \frac{2}{\sqrt{3}} t_{\mathbf{k}} \cos\left(\frac{\phi_{\mathbf{k}} + 2\pi\alpha}{3}\right) + \frac{\epsilon_{\rm d} - \epsilon_{\rm p}}{3}, \tag{51}$$

for $\alpha = 0$, 1 and 2, where

$$t_{\mathbf{k}} = \sqrt{|\eta^x_{\mathbf{k}}|^2 + |\eta^y_{\mathbf{k}}|^2 + (\eta^p_{\mathbf{k}})^2 + (\epsilon_{\rm d} - \epsilon_{\rm p})^2/3}, \tag{52}$$

$$\phi_{\mathbf{k}} = \frac{\pi}{2} + \text{sign}(s_{\mathbf{k}}) \left(\frac{\pi}{2} - \arctan\sqrt{|1 - 4t^6_{\mathbf{k}}/(27 s^2_{\mathbf{k}})|}\right), \tag{53}$$

$$s_{\mathbf{k}} = (\epsilon_{\rm d} - \epsilon_{\rm p}) \left(\frac{(\epsilon_{\rm d} - \epsilon_{\rm p})^2}{27} - \frac{t^2_{\mathbf{k}}}{3} + (\eta^p_{\mathbf{k}})^2\right) + \eta^p_{\mathbf{k}} (\eta^x_{\mathbf{k}} \eta^{y*}_{\mathbf{k}} + \eta^{x*}_{\mathbf{k}} \eta^y_{\mathbf{k}}), \tag{54}$$

where $\eta^x_{\mathbf{k}} = 2it_{\rm dp} \sin(k_x/2)$, $\eta^y_{\mathbf{k}} = 2it_{\rm dp} \sin(k_y/2)$, and $\eta^p_{\mathbf{k}} = -4t_{\rm pp} \sin(k_x/2) \sin(k_y/2)$. $\epsilon^\alpha_{\mathbf{k}}$ for $\alpha = 0, 1, 2$ is the dispersion relation of the upper, lower and middle band, respectively. We examine the doped case within the hole picture where the lowest band is occupied up to the Fermi energy μ. The effective interaction is

$$V_{\mathbf{k}\mathbf{k}'} = \frac{U_{\rm d}}{N} + \frac{U^2_{\rm d}}{N} \chi^{\rm dd}(\mathbf{k} + \mathbf{k}'), \tag{55}$$

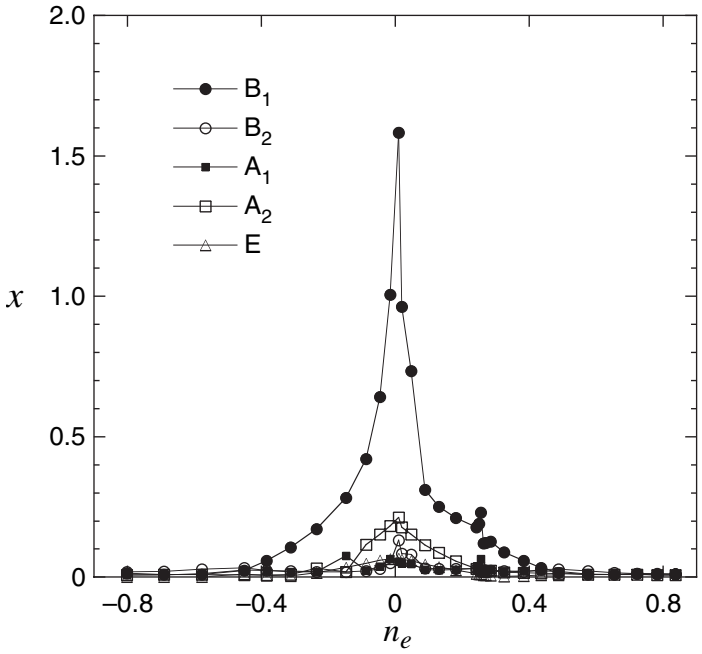

Figure 14. x as a function of the carrier density n_e for the square lattice d–p model: $n_e > 0$ for hole doping and $n_e < 0$ for electron doping.

where

$$\chi^{dd}(\mathbf{q}) = \frac{1}{N}\sum_{\mathbf{p}}\sum_{\alpha\beta} w^{\alpha}_{\mathbf{q}+\mathbf{p}} \frac{f^{\alpha}_{\mathbf{q}+\mathbf{p}} - f^{\beta}_{\mathbf{p}}}{\epsilon^{\beta}_{\mathbf{p}} - \epsilon^{\alpha}_{\mathbf{q}+\mathbf{p}}} w^{\beta}_{\mathbf{p}}. \tag{56}$$

Here $f^{\alpha}_{\mathbf{k}}$ is the Fermi distribution function,

$$f^{\alpha}_{\mathbf{k}} = (e^{\beta(\epsilon^{\alpha}_{\mathbf{k}} - \mu)} + 1)^{-1}. \tag{57}$$

The weighting factor of d electrons $w^{\alpha}_{\mathbf{k}}$ is defined as

$$w^{\alpha}_{\mathbf{k}} = \frac{(\eta^{p}_{\mathbf{k}} - \epsilon^{\alpha}_{\mathbf{k}})(\eta^{p}_{\mathbf{k}} + \epsilon^{\alpha}_{\mathbf{k}})}{(\epsilon^{\beta}_{\mathbf{k}} - \epsilon^{\alpha}_{\mathbf{k}})(\epsilon^{\alpha}_{\mathbf{k}} - \epsilon^{\gamma}_{\mathbf{k}})}, \tag{58}$$

where α, β and γ are different from each other. The gap equation is

$$\Delta_k = -\sum_{k'} w_k V^{dd}_{kk'} w_{k'} \Delta_{k'} \frac{1}{2E_{k'}}, \tag{59}$$

where $w_k = w^1_{\mathbf{k}}$ and $E_k = \sqrt{\xi^2_k + \Delta^2_k}$ for the lowest-band dispersion $\xi_k = \epsilon^1_k - \mu$.

The d-wave pairing is predominant over the whole range in the parameter space as is shown in figure 14. In particular, $d_{x^2-y^2}$-wave pairing is stable near half-filling. Although the extended s-wave pairing is possible in the narrow region near half filling in the Gutzwiller variational Monte Carlo study [14], we have no chance of s-wave SC within the weak-coupling perturbation theory. The phase diagram for the d–p model is shown in figure 15.

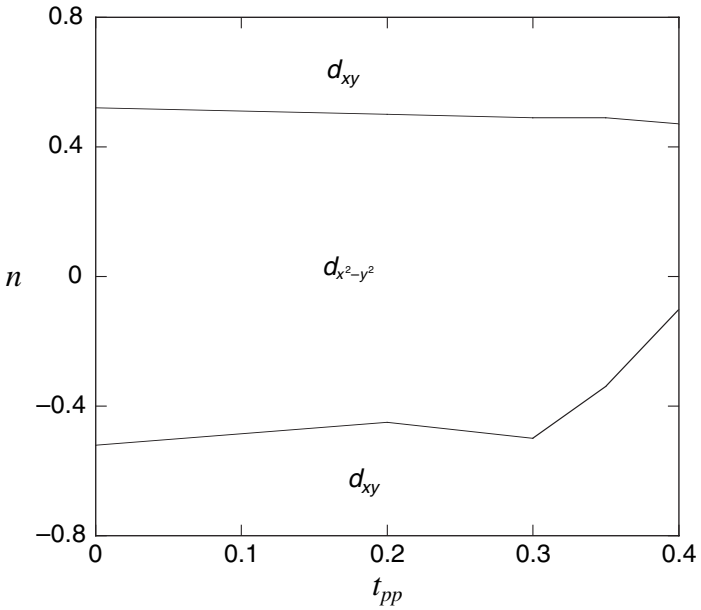

Figure 15. Phase diagram for the three-band d–p model in the plane of the carrier number n and $t_{\rm pp}$ in the range of $0 \leqslant t_{\rm pp} \leqslant 0.4$. We set $\epsilon_{\rm p} - \epsilon_{\rm d} = 2$ and $t_{\rm dp} = 1$. $n = 0$ indicates half filling, and the positive and negative n are for hole doping and electron doping, respectively.

5. Summary

We have examined the phase diagram with respect to pairing symmetry on the basis of the 2D Hubbard model. The weak coupling formulation is convenient to investigate the phase diagram in detail. The results are almost consistent with the strong-coupling perturbation theory. We summarize the results as follows.

1. The d-wave pairing is stable near half filling for the square lattice and the anisotropic square lattice.
2. The gap function has a maximum at the van Hove singularity. As the second neighbor transfer t' increases, the energy of the van Hove singularity decreases. For large $t' = -0.3$ to ~ -0.4, the optimal doping is more than 25% doping, i.e. $n_{\rm e} < 0.75$. For small third neighbor transfer t'' the situation remains the same. The large $-t'$ is assigned to several high-temperature cuprates to fit the angle resolved photoemission spectroscopy (ARPES) data or the Fermi surface obtained by the band structure calculations. Most of them, however, have optimum critical temperature in the range of $0.8 < n_{\rm e} < 0.85$. Thus, the weak coupling analysis suggests that we must consider other electronic or lattice interactions, or reexamine the band parameters t' and t''. Recent ARPES studies have reported the band structure which is well fitted using rather smaller t' such as $t' \sim -0.2$ by our analysis.
3. The predictions of the weak-coupling theory are almost consistent with the variational Monte Carlo method. An effective interaction to induce SC is possibly the simple $\chi(\mathbf{q})$ with renormalization in the Gutzwiller variational theory.

4. For the d–p model, the d-wave pairing is predominant in a wide range and the phase diagram is almost symmetric between electron and hole dopings. Although the pairing symmetry in the electron-doped cuprates is controversial, only the d-wave pairing is possible near half-filling in the weak-coupling formulation.

Acknowledgments

This work was supported by grants-in-aid for Scientific Research from the Ministry of Education, Culture, Sports, Science and Technology of Japan. Some of the numerical calculations were performed at the facilities of the Supercomputer Center of the Institute for Solid State Physics, University of Tokyo.

I sincerely thank J Kondo, K Yamaji and S Koikegami for fruitful discussions.

Appendix. Higher-order corrections

In the appendix, we examine higher-order corrections to x. If the third-order terms have an effect to reduce the exponent x, the results obtained using the second-order perturbation have a possibility to become unstable as U increases. It is not an easy task to derive an effective Hamiltonian up to the third order of the interaction using the canonical transformation. The gap equation up to the third order of U has been obtained using the perturbative expansion for the Hubbard model [41, 42]. The Green's functions satisfy the Dyson equations:

$$G(\mathbf{k}, \mathrm{i}\epsilon_n) = G_0(\mathbf{k}, \mathrm{i}\epsilon_n) + G_0(\mathbf{k}, \mathrm{i}\epsilon_n)\Sigma_n(\mathbf{k}, \mathrm{i}\epsilon_n)G(\mathbf{k}, \mathrm{i}\epsilon_n) + G_0(\mathbf{k}, \mathrm{i}\epsilon_n)\Sigma_a(\mathbf{k}, \mathrm{i}\epsilon_n)F^*(\mathbf{k}, \mathrm{i}\epsilon_n), \tag{A.1}$$

$$F(\mathbf{k}, \mathrm{i}\epsilon_n) = G_0(\mathbf{k}, \mathrm{i}\epsilon_n)\Sigma_n(\mathbf{k}, \mathrm{i}\epsilon_n)F(\mathbf{k}, \mathrm{i}\epsilon_n) - G_0(\mathbf{k}, \mathrm{i}\epsilon_n)\Sigma_a(\mathbf{k}, \mathrm{i}\epsilon_n)G(-\mathbf{k}, -\mathrm{i}\epsilon_n), \tag{A.2}$$

where $\epsilon_n = (2n+1)\pi k_\mathrm{B}T$ is the Matsubara frequency, and Σ_n (Σ_a) is the normal (anomalous) self-energy. G_0 is the free-electron Green's function: $G_0(\mathbf{k}, \mathrm{i}\epsilon_n) = (\mathrm{i}\epsilon_n - \xi_k)^{-1}$. Since we are interested in the third-order contributions, Σ_n (of the order of U^2) is neglected as follows:

$$G(\mathbf{k}, \mathrm{i}\epsilon_n) = -\frac{\mathrm{i}\epsilon_n + \xi_k}{\epsilon_n^2 + \xi_k^2 + |\Sigma_a(\mathbf{k}, \mathrm{i}\epsilon_n)|^2}, \tag{A.3}$$

$$F(\mathbf{k}, \mathrm{i}\epsilon_n) = -\frac{\Sigma_a(\mathbf{k}, \mathrm{i}\epsilon_n)}{\epsilon_n^2 + \xi_k^2 + |\Sigma_a(\mathbf{k}, \mathrm{i}\epsilon_n)|^2}. \tag{A.4}$$

The equation for the anomalous self-energy is

$$\begin{aligned}\Sigma_a(\mathbf{k}, \mathrm{i}\epsilon_n) = {} & \frac{1}{\beta N}\sum_{k', \epsilon_{n'}}[U + U^2\chi_0(\mathbf{k}+\mathbf{k}', \mathrm{i}\epsilon_n + \mathrm{i}\epsilon_{n'}) + 2U^3\chi_0(\mathbf{k}+\mathbf{k}', \mathrm{i}\epsilon_n + \mathrm{i}\epsilon_{n'})^2]F(\mathbf{k}', \mathrm{i}\epsilon_{n'}) \\ & + U^3\frac{1}{\beta^2 N^2}\sum_{k', \epsilon_{n'}, p, \epsilon_\ell} G_0(\mathbf{k}', \mathrm{i}\epsilon_{n'})[\chi_0(\mathbf{k}+\mathbf{k}', \mathrm{i}\epsilon_n + \mathrm{i}\epsilon_{n'}) \\ & - \phi_0(\mathbf{k}+\mathbf{k}', \mathrm{i}\epsilon_n + \mathrm{i}\epsilon_{n'})]G_0(\mathbf{k}+\mathbf{k}'+\mathbf{p}, \mathrm{i}\epsilon_n + \mathrm{i}\epsilon_{n'} + \mathrm{i}\epsilon_\ell)F(\mathbf{p}, \mathrm{i}\epsilon_\ell) \\ & + U^3\frac{1}{\beta^2 N^2}\sum_{k', \epsilon_{n'}, p, \epsilon_\ell} G_0(\mathbf{k}', \mathrm{i}\epsilon_{n'})[\chi_0(-\mathbf{k}+\mathbf{k}', -\mathrm{i}\epsilon_n + \mathrm{i}\epsilon_{n'}) \\ & - \phi_0(-\mathbf{k}+\mathbf{k}', -\mathrm{i}\epsilon_n + \mathrm{i}\epsilon_{n'})]G_0(-\mathbf{k}+\mathbf{k}'-\mathbf{p}, -\mathrm{i}\epsilon_n + \mathrm{i}\epsilon_{n'} - \mathrm{i}\epsilon_\ell)F(\mathbf{p}, \mathrm{i}\epsilon_\ell),\end{aligned} \tag{A.5}$$

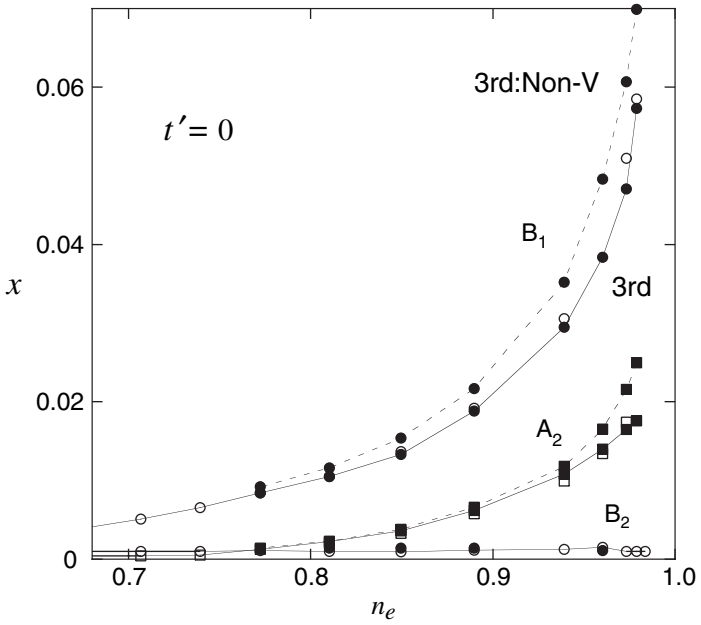

Figure A1. The exponent x for the second-order (open symbols) and third-order (solid symbols) perturbation in U. We set $U/t = 0.1$. The symbol Non-V indicates the results obtained without vertex corrections.

for $\beta = 1/k_{\mathrm{B}}T$. The second and third terms originate from the vertex corrections. $\chi_0(\mathbf{q}, \mathrm{i}\omega_m)$ and $\phi_0(\mathbf{q}, \mathrm{i}\omega_m)$ are defined as

$$\chi_0(\mathbf{q}, \mathrm{i}\omega_m) = -\frac{1}{N}\sum_k \frac{f(\xi_k) - f(\xi_{k+q})}{\mathrm{i}\omega_m + \xi_k - \xi_{k+q}}, \tag{A.6}$$

$$\phi_0(\mathbf{q}, \mathrm{i}\omega_m) = -\frac{1}{N}\sum_k \frac{f(\xi_k) - f(-\xi_{-k+q})}{\mathrm{i}\omega_m - \xi_k - \xi_{-k+q}}, \tag{A.7}$$

where $\omega_m = 2\pi m k_{\mathrm{B}}T$. We assume that Σ_a is small and that we can neglect the ϵ-dependence since we consider the small-U limit. We set $\Delta_{\mathbf{k}} = \Sigma_a(\mathbf{k}, \epsilon_n = 0)$, then the equation for $\Delta_{\mathbf{k}}$ is derived. We show the results in figure A1 for $U/t = 0.1$ on the square lattice. The exponent x slightly decreases due to the third-order corrections. There is a cancellation among the third-order terms. As has been shown in the literature [41], the vertex corrections reduce the exponents x and T_{c} compared to those without vertex corrections.

References

[1] Dagotto E 1994 *Rev. Mod. Phys.* **66** 763
[2] Scalapino D J 1990 *High Temperature Superconductivity—the Los Alamos Symposium—1989 Proceedings* ed K S Bedell, D Coffey, D E Deltzer, D Pines and J R Schrieffer (Redwood City, CA: Addison-Wesley) p 314
[3] Anderson P W 1997 *The Theory of Superconductivity in the High-T_c Cuprates* (Princeton, NJ: Princeton University Press)
[4] Stewart G R 1984 *Rev. Mod. Phys.* **56** 755

[5] Lee P A, Rice T M, Serene J W, Sham L J and Wilkins J W 1986 *Comments Condens. Matter Phys.* **12** 99
[6] Ott H R 1987 *Prog. Low Temp. Phys.* **11** 215
[7] Maple M B 2000 *Handbook on the Physics and Chemistry of Rare Earths* vol 30 (Amsterdam: North-Holland, Elsevier)
[8] Loh E Y, Gubernatis J E, Scalettar R T, White S R, Scalapino D J and Sugar R L 1990 *Phys. Rev.* B **41** 9301
[9] Moreo A, Scalapino D J and Dagotto E 1991 *Phys. Rev.* B **56** 11442
[10] Wheatley J 1993 *Solid State Commun.* **88** 593
[11] Nakanishi T, Yamaji K and Yanagisawa T 1997 *J. Phys. Soc. Japan* **66** 294
[12] Yamaji K, Yanagisawa T, Nakanishi T and Koike S 1998 *Physica* C **304** 225
[13] Neumayr A and Metzner W 2003 *Phys. Rev.* B **67** 035112
[14] Yanagisawa T, Koike S and Yamaji K 2001 *Phys. Rev.* B **64** 184509
Yanagisawa T, Koike S and Yamaji K 2003 *Phys. Rev.* B **67** 132408
[15] Yanagisawa T, Koike S and Yamaji K 2002 *J. Phys.: Condens. Matter* **14** 21
[16] Miyazaki M, Yamaji K and Yanagisawa T 2004 *J. Phys. Soc. Japan* **73** 1643
[17] Miyake K, Schmidt-Rink S and Varma C M 1986 *Phys. Rev.* B **34** 6554
[18] Scalapino D J, Loh E and Hirsch J E 1986 *Phys. Rev.* B **34** 8190
[19] Kondo J 2001 *J. Phys. Soc. Japan* **70** 808
[20] Hlubina R 1999 *Phys. Rev.* B **59** 9600
[21] Schauerte T and van Dongen P G J 2002 *Phys. Rev.* B **65** 081105
[22] Kondo J private communication
[23] Singh D J and Pickett W E 1992 *Physica* C **203** 193
[24] Singh D J 1993 *Physica* C **212** 228
[25] Tohyama T and Maekawa S 2000 *Supercond. Sci. Technol.* **13** 17
[26] Harris J M, Shen Z X, White P J, Marshall D S and Schabel M C 1996 *Phys. Rev.* B **54** R15665
[27] McElory K, Simmonds R W, Hoffman J E, Lee D-H, Orenstein J, Eisaki H, Uchida S and Davis J C 2003 *Nature* **422** 592
[28] Feng D L *et al* 2001 *Phys. Rev. Lett.* **86** 5550
[29] Hussey N E, Abdel-Jawad M, Carrington A, Mackenzie A P and Ballcas L 2003 *Nature* **425** 814
[30] Yamaji K 2007 private communication
[31] Maeno Y, Hashimoto H, Yoshida K, Nishizaki S, Fujita T, Bednorz J G and Lichtenberg F 1994 *Nature* **372** 532
[32] Koikegami S, Yoshida Y and Yanagisawa T 2003 *Phys. Rev.* B **67** 134517
[33] McKenzie R H 1997 *Science* **278** 820
[34] McKenzie R H 1998 *Comments Condens. Matter Phys.* **18** 309
[35] Miyanaga K, Kanoda K and Kasamoto A 2004 *Chem. Phys.* **104** 5635
[36] Kondo H and Moriya T 2004 *J. Phys. Soc. Japan* **73** 812
[37] Koikegami S and Yanagisawa T 2001 *J. Phys. Soc. Japan* **70** 3499
Koikegami S and Yanagisawa T 2002 *J. Phys. Soc. Japan* **71** 671
[38] Yanagisawa T, Koikegami S, Shibata H, Kimura S, Kashiwaya S, Sawa A, Matsubara N and Takita K 2001 *J. Phys. Soc. Japan* **70** 2833
[39] Sato T, Kamiyama T, Takahashi T, Kurahashi K and Yamada K 2001 *Science* **291** 1517
[40] Chen C-T, Seneor P, Yeh N-C, Vasquez R P, Bell L D, Jung C U, Kim J Y, Park M-S, Kim H-J and Lee S-I 2002 *Phys. Rev. Lett.* **88** 227002
[41] Jujo T, Koikegami S and Yamada K 1999 *J. Phys. Soc. Japan* **68** 1331
[42] Nomura T and Yamada K 2001 *J. Phys. Soc. Japan* **70** 2694